environments

Article

Degradation of Multicomponent Tannery Dye Mixtures by Electrochemical Advanced Oxidation Processes

Yessica G. López-Duran [1], Martín O. A. Pacheco-Álvarez [1], Silvia Gutiérrez-Granados [1], Oracio Serrano [1], Patricio Espinoza [2], Enric Brillas [3] and Juan M. Peralta-Hernández [1,*]

[1] Lab.11-Laboratorio de Medio Ambiente y Electroquímica (LMAE), Departamento de Química-DCNE, Universidad de Guanajuato, Cerro de la Venada s/n, Pueblito de Rocha, Guanajuato 36040, Mexico; oraciosinh@ugto.mx (O.S.)
[2] Escuela de Ciencias Químicas, Pontificia Universidad Católica del Ecuador, Avenida 12 de Octubre y Roca, Quito P.O. Box 1701-2184, Ecuador; pespinoza646@puce.edu.ec
[3] Departament de Ciència de Materials i Química Física, Facultat de Química, Universitat de Barcelona, Martí i Franquès 1-11, CP 08028 Barcelona, Spain; brillas@ateneu.ub.edu
* Correspondence: juan.peralta@ugto.mx

Abstract

Industrial effluents containing persistent synthetic dyes represent an important environmental challenge because of their high chemical stability, low biodegradability, and potential adverse effects on aquatic ecosystems. This study evaluates electrochemical advanced oxidation processes (EAOPs) as remediation strategies for dye-contaminated tanery dyes, with particular emphasis on conditions representative of complex industrial effluents. Electrochemical oxidation (EOx), electro-Fenton (EF), and photoelectro-Fenton (PEF) processes using boron-doped diamond (BDD) electrodes were comparatively investigated for the degradation of Violet S4B and a multicomponent mixture containing Violet S4B, Brown DR, and Black NT2. The effects of current density and pollutant concentration were assessed through discoloration, pseudo-first-order kinetics, chemical oxygen demand (COD) removal, and HPLC analysis of oxidation intermediates. For the multicomponent system, PEF achieved approximately 99% discoloration after 120 min, compared with nearly 97% for EF and 95% for EOx, with apparent rate constants increasing in the order EOx < EF < PEF. More importantly, COD analysis demonstrated extensive mineralization during PEF treatment, while HPLC revealed negligible accumulation of oxalic acid, indicating effective oxidation of refractory intermediates. The results demonstrate that combining anodic oxidation, electrochemically generated Fenton chemistry, and photo-assisted reactions enhances the remediation of complex dye mixtures. These findings support BDD-based EAOPs, particularly PEF, as promising technologies for reducing persistent organic pollution associated with tannery dye solutions.

Keywords: environmental remediation; electrochemical advanced oxidation processes; boron-doped diamond; photoelectro-Fenton; multicomponent dye mixtures; water pollution

Check for updates

Academic Editors: Heriberto Cruz-Martínez, Fabiola Lango-Reynoso, Virginia Hernández-Montoya and Lucija Radetić

Received: 8 August 2026
Revised: 3 September 2026
Accepted: 10 September 2026
Published: 11 September 2026

Copyright: © 2026 by the authors. Licensee MDPI, Basel, Switzerland. This article is an open access article distributed under the terms and conditions of the Creative Commons Attribution (CC BY) license.

1. Introduction

Industrial wastewaters generated by textile, leather, pharmaceutical, and related manufacturing sectors represent an important source of persistent organic pollution in aquatic environments because they frequently contain recalcitrant contaminants that are poorly removed by conventional treatment technologies. Among these industrial activities,

leather manufacturing is of particular environmental concern due to the large volumes of wastewater generated and the discharge of synthetic dyes and auxiliary chemicals during retanning, dyeing, and oiling operations. The persistence and chemical stability of these compounds can contribute to the deterioration of receiving water bodies, emphasizing the need for effective treatment strategies capable of reducing the organic pollutant load before wastewater discharge or reuse. These effluents exhibit high chemical stability and low biodegradability, limiting the effectiveness of conventional treatments and promoting the persistence of contaminants in aquatic environments. Consequently, developing efficient oxidation technologies capable of enhancing pollutant degradation and mineralization has become an important challenge for the sustainable management of tannery wastewaters. In this context, advanced oxidation processes (AOPs) have attracted considerable attention because of their ability to generate highly reactive species for the degradation of refractory organic contaminants and improved treatment performance [1,2].

Beyond pollutant removal, advanced treatment technologies play an important role in promoting sustainable industrial practices and circular economy strategies. In the tannery industry, efficient treatment of dye-containing effluents enables water reuse and recirculation, reducing both freshwater consumption and wastewater generation. Therefore, advanced oxidation processes capable of treating complex dye mixtures represent a promising approach for improving the environmental sustainability and resource efficiency of leather production systems [3].

Synthetic dyes used in leather processing are designed to exhibit high color intensity together with excellent resistance to light, oxidation, and biodegradation [4]. Although these properties are essential for producing durable leather products, they also make these compounds highly persistent in wastewater and difficult to remove by conventional treatment technologies. Even at low concentrations, dyes adversely affect water quality by reducing light penetration, disrupting aquatic photosynthesis, and generating toxic or mutagenic transformation products during degradation [5]. Consequently, the development of effective technologies for degrading these recalcitrant contaminants remains a major research priority in environmental and chemical engineering [6].

Specific discharge limits for individual industrial dyes such as Violet S4B, Brown DR, and Black NT2 are generally not established. In Mexico, NOM-001-SEMARNAT-2021 regulates colored wastewater through the true-color parameter, establishing maximum spectral absorption coefficients of 7.0, 5.0, and 3.0 m^{-1} at 436, 525, and 620 nm, respectively [7]. Although concentrations of these specific commercial dyes in real tannery effluents have not been systematically reported, dye-containing industrial wastewaters commonly exhibit concentrations of 10–50 mg L^{-1}, while values of 100–200 mg L^{-1} and ranges up to 10–250 mg L^{-1} have also been reported for different textile and dyeing operations [8]. Thus, the concentrations evaluated in this study (50–150 mg L^{-1}) are within environmentally relevant pollutant loads reported for industrial dye-containing effluents.

Although electrochemical advanced oxidation processes (EAOPs) have been extensively investigated, most studies evaluate their performance using single model pollutants under simplified laboratory conditions. While these investigations provide valuable mechanistic insights, they do not adequately represent industrial wastewaters, where multiple organic contaminants simultaneously compete for reactive oxygen species and active electrode sites. Consequently, the performance of EAOPs under representative multicomponent conditions remains insufficiently understood, limiting the extrapolation of laboratory-scale results to real industrial applications.

Conventional technologies, including coagulation–flocculation, adsorption, membrane filtration, and biological treatment, have been widely employed for dye-containing wastewaters. However, these methods exhibit significant limitations when treating persistent

organic contaminants. Physical processes generally transfer pollutants from the aqueous phase to another medium without destruction, generating secondary waste that requires further management [9]. Likewise, biological treatment is often ineffective because of the high chemical stability and low biodegradability of synthetic dyes [10]. Consequently, more efficient oxidation technologies capable of achieving effective contaminant degradation and mineralization are required.

Advanced oxidation processes (AOPs) have emerged as effective technologies for the treatment of recalcitrant organic contaminants in water and wastewater. Their performance is based on the in situ generation of highly reactive species, particularly hydroxyl radicals ($^{\bullet}$OH), which possess high oxidation potential and react non-selectively with a broad range of organic compounds [11]. These reactions promote the breakdown of complex molecular structures into smaller intermediates and, under appropriate operating conditions, their eventual mineralization to carbon dioxide, water, and inorganic ions.

Among advanced oxidation technologies, electrochemical advanced oxidation processes (EAOPs) have attracted considerable attention because of their operational flexibility and suitability for on-site wastewater treatment. In these systems, oxidizing species are generated either directly at the electrode surface or indirectly through electrochemically produced reagents. A key advantage of EAOPs is the ability to regulate reactive species generation by controlling the applied current density (j) or electrode potential, providing precise control over the oxidation process [12].

Electrooxidation (EOx) is the simplest EAOP for the degradation of organic contaminants. In this process, water oxidation at the anode generates adsorbed hydroxyl radicals that react with pollutants in solution [13]. Process performance largely depends on the anode material, with boron-doped diamond (BDD) electrodes being among the most effective because of their wide potential window, high chemical stability, low background current, and ability to generate weakly physisorbed hydroxyl radicals (BDD($^{\bullet}$OH)) according to Equation (1) [14]. These properties promote efficient contaminant oxidation while minimizing electrode fouling.

$$\mathrm{BDD} + \mathrm{H_2O} \rightarrow \mathrm{BDD}(^{\bullet}\mathrm{OH}) + \mathrm{H^+} + \mathrm{e^-} \quad (1)$$

Electro-Fenton (EF) is another widely studied EAOP based on the electrochemical generation of hydrogen peroxide (H_2O_2) and its catalytic activation by ferrous ions. In this process, H_2O_2 is continuously produced at the cathode through the reduction of dissolved oxygen, as described by Equation (2) [15]:

$$\mathrm{O_2} + 2\mathrm{H^+} + 2\mathrm{e^-} \rightarrow \mathrm{H_2O_2} \quad (2)$$

The electrogenerated H_2O_2 subsequently reacts with ferrous ions through the classical Fenton reaction to produce hydroxyl radicals ($^{\bullet}$OH), as described by Equation (3) [16]:

$$\mathrm{Fe^{2+}} + \mathrm{H_2O_2} \rightarrow \mathrm{Fe^{3+}} + \mathrm{OH^-} + {}^{\bullet}\mathrm{OH} \quad (3)$$

The electrochemical reduction of ferric to ferrous ions, according to Equation (4), enables continuous Fenton reagent regeneration and sustained hydroxyl radical production [17]. This feature enhances process efficiency and has enabled the successful application of EF to the treatment of dyes, pharmaceuticals, pesticides, and other industrial contaminants [18].

$$\mathrm{Fe^{3+}} + \mathrm{e^-} \rightarrow \mathrm{Fe^{2+}} \quad (4)$$

The efficiency of the electro-Fenton process can be further enhanced by coupling it with irradiation, giving rise to the photoelectro-Fenton (PEF) process. In this hybrid

system, UVA or solar radiation promotes the photoreduction of ferric complexes, according to Equation (5), increasing hydroxyl radical ($^{\bullet}$OH) production and improving process performance [19].

$$Fe(OH)^{2} + h\nu \rightarrow Fe^{2+} + {}^{\bullet}OH \quad (5)$$

In addition, irradiation promotes the photodegradation of carboxylate intermediates that are more resistant to electrochemical oxidation, according to the general reaction described by Equation (6) [20]. This synergistic effect accelerates mineralization and enhances the overall performance of the PEF process compared with EF alone.

$$Fe^{3+}(RCOO^{-})^{2+} + h\nu \rightarrow Fe^{2+} + CO_2 + R^{\bullet} \quad (6)$$

Despite their proven effectiveness, systematic comparisons of electrooxidation (EOx), electro-Fenton (EF), and photoelectro-Fenton (PEF) under identical operating conditions remain limited. Such evaluations are essential for elucidating the relative contributions of electrochemical and photochemical pathways and for identifying the most suitable treatment strategy for complex wastewaters. Kinetic analysis provides a quantitative basis for comparing process performance by determining apparent degradation rate constants under different operating conditions, thereby facilitating the evaluation and optimization of EAOPs [21].

This study presents a comparative evaluation of electrooxidation (EOx), electro-Fenton (EF), and photoelectro-Fenton (PEF) for the treatment of a representative tannery dye and a multicomponent dye mixture using boron-doped diamond (BDD) electrodes [22]. The influence of key operating parameters, particularly current density and initial dye concentration, was systematically investigated, whereas the Fe^{2+} concentration employed in the EF and PEF experiments was selected based on previous optimization studies. Process performance was assessed through discoloration, chemical oxygen demand (COD) removal, and pseudo-first-order kinetic analysis [23]. Particular emphasis was placed on comparing the contributions of electrochemical and photo-assisted oxidation pathways under identical operating conditions. The results provide environmentally relevant insights into the performance of EAOPs for the remediation of complex dye-contaminated waters and their potential application to the treatment of tannery effluents containing persistent organic pollutants.

2. Materials and Methods

2.1. Chemicals

The model dye used in this study was Violet S4B (Crystal Violet), a synthetic dye commonly employed during leather dyeing in the tannery industry (Pequeño Curtidor de León, S.A. de C.V. (PCL, León, Guanajuato, Mexico)). In addition, a representative multicomponent dye mixture was prepared to simulate industrial effluents, containing Violet S4B, Brown DR, and Black NT2 at equal concentrations (50 mg L^{-1} each; total concentration 150 mg L^{-1}) in 50 mM Na_2SO_4 at pH 3.0. The initial pH was adjusted to 3.0 for all experiments to provide a common operating condition for comparison among EOx, EF, and PEF and, particularly, to ensure favorable conditions for the Fe^{2+}/Fe^{3+} catalytic cycle involved in the Fenton-based processes. It should be emphasized that the dye solutions investigated here were model systems rather than actual tannery wastewater. Consequently, the selected pH does not represent the native pH of tannery effluents, which may be alkaline depending on the processing stage. Application of EF or PEF to alkaline tannery wastewater would therefore require pH adjustment as a pretreatment step, and the associated chemical consumption should be considered when evaluating practical implementation.

Comparative experiments with the dye mixture were performed using a BDD plate anode at 70 mA cm^{-2}. Ferrous sulfate heptahydrate ($FeSO_4 \cdot 7H_2O$, ≥99%, Merck KGaA (Darmstadt, Germany) was used as the Fe^{2+} source in the EF and PEF processes. Sodium sulfate (Na_2SO_4, ≥99%, Merck KGaA (Darmstadt, Germany)) served as the supporting electrolyte, while sulfuric acid (H_2SO_4, 95–98%, Fisher Scientific S.L. (Alcobendas, Madrid, Spain)) and sodium hydroxide (NaOH, ≥98%, Merck, Germany) were used for pH adjustment. All reagents were analytical grade and used without further purification.

Solutions were prepared with untreated tap water to better represent practical model systems treatment conditions, as described previously [24]. Continuous air bubbling (≈3 L min^{-1}) supplied the dissolved oxygen required for H_2O_2 electrogeneration using an aquarium air pump (SunSun YT-302C air pump (Sensen Group Co., Ltd., Zhoushan, China), 3 W) connected to a porous air-stone diffuser located at the bottom of the reactor, ensuring adequate oxygen transfer and electrolyte mixing.

Fresh dye solutions were prepared immediately before each experiment. The Fe^{2+} concentration employed in the EF and PEF experiments was selected from preliminary optimization studies reported previously [25].

2.2. Electrochemical Reactor

Electrochemical experiments were conducted in a laboratory-scale batch reactor with a working volume of 500 mL. The reactor consisted of a cylindrical borosilicate glass vessel to allow efficient light transmission during the PEF experiments. The electrochemical cell consisted of a 5 cm^2 BDD plate anode (METAKEM GmbH (Usingen, Germany)) and a stainless-steel cathode for the EOx process. In the EF and PEF experiments, both electrodes were of BDD. The electrodes were arranged in a parallel configuration and connected to a regulated B&K Precision 1670A DC power supply (B&K Precision Corporation, Yorba Linda, CA, USA) for accurate control of the applied current [24].

During all the experiments, the dye solution was continuously stirred to enhance mass transfer between the bulk solution and the electrode surfaces. All electrochemical treatments were performed at room temperature [26].

For the PEF experiments, the electrochemical system was coupled with an ultraviolet irradiation source. A UV-A lamp (365 nm, 15 W, Philips, model TL-D 15W/08, Signify Netherlands B.V. (Philips), Eindhoven, The Netherlands) was positioned approximately 10 cm above the reactor, providing uniform illumination of the reaction medium with an average irradiance of about 20–25 W m^{-2}. The complete reactor arrangement is shown in Figure 1. Similar irradiation conditions have been reported in photo-Fenton and PEF processes for dye degradation, as described in previous studies [27].

2.3. Analytical Methods

Dye degradation during the electrochemical treatments was monitored by UV–Vis spectrophotometry. Before the experiments, full spectra (200–800 nm) were recorded using a double-beam UV–Vis spectrophotometer (CINTRA 1010, GBC Scientific Equipment Pty Ltd., Braeside, Victoria, Australia) to determine the maximum absorption wavelength (λ_{max}), which was subsequently used to monitor dye concentration throughout the experiments. Aliquots were collected at predetermined intervals (10–20 min), filtered through 0.45 μm PTFE syringe filters (MilliporeSigma, Burlington, MA, USA), and immediately analyzed. The relative dye concentration (C/C_0) was calculated from the corresponding absorbance values according to the Beer–Lambert law.

Mineralization was evaluated by measuring the chemical oxygen demand (COD) using the dichromate method (Standard Methods 5220D). COD measurements were performed with a digestion reactor (HACH DRB200, Hach Company, Loveland, CO, USA)

and a multiparameter photometer (HACH DR6000, Hach Company, Loveland, CO, USA). Samples collected before and after treatment were used to determine the extent of organic matter removal.

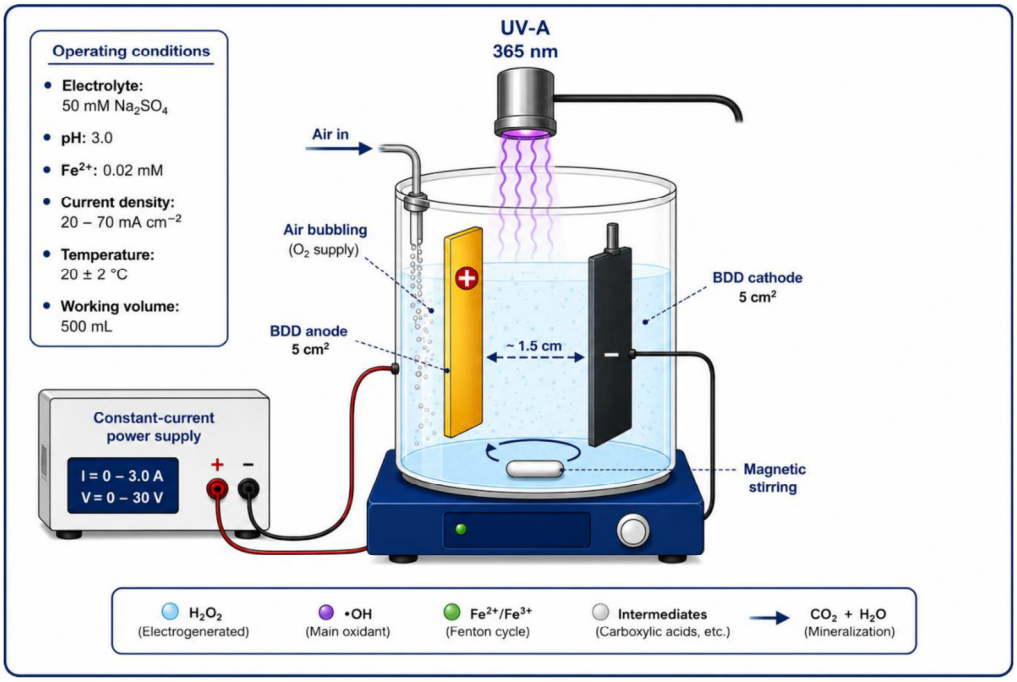


Figure 1. Schematic diagram of the laboratory-scale batch photoelectrochemical reactor employed for the EOx, EF, and PEF experiments. The reactor consisted of a 500 mL borosilicate glass cell equipped with BDD electrodes (5 cm^2), UV-A irradiation (365 nm), continuous air bubbling, magnetic stirring, and a constant-current DC power supply.

Selected samples were further analyzed by high-performance liquid chromatography (HPLC) to identify intermediate degradation products. Analyses were carried out using an Agilent 1260 Infinity system (Agilent Technologies, Inc., Santa Clara, CA, USA) equipped with a diode-array detector (DAD). Carboxylic acids were separated by ion-exclusion chromatography using a Bio-Rad Aminex HPX-87H column, 300 × 7.8 mm, (Bio-Rad Laboratories, Inc., Hercules, CA, USA) with 4 mM H_2SO_4 as the mobile phase at a flow rate of 0.6 mL min^{-1}. The injection volume was 20 µL, and the column temperature was maintained at 35 °C.

2.4. Experimental Procedure

Electrochemical degradation experiments were performed using aqueous dye solutions prepared with untreated tap water. The initial pH was adjusted to 3.0 using dilute H_2SO_4 or NaOH before each experiment. The electrolyte was transferred to the electrochemical reactor and maintained under continuous stirring throughout the treatment.

EOx experiments were conducted under galvanostatic conditions by applying a constant current density in a batch reactor for the desired electrolysis time. For EF experiments, Fe^{2+} was added before electrolysis, while continuous air bubbling was supplied to promote the electrogeneration of H_2O_2. PEF experiments were carried out under the same operating conditions as EF, with the addition of UVA irradiation.

The influence of the applied current density and initial dye concentration on process performance was systematically evaluated. The Fe^{2+} concentration employed in the EF and PEF experiments was fixed at the value selected from previous optimization studies [28].

3. Results and Discussion: Environmental Remediation of Tannery Dye-Contaminated Water

3.1. UV–Vis Characterization of Violet S4B

The UV–Vis absorption spectrum of the initial Violet S4B solution shown in Figure 2 was recorded prior to the electrochemical experiments exclusively to characterize its initial spectroscopic behavior and identify the maximum absorption wavelength (λ_{max}) used for subsequent discoloration monitoring. Therefore, Figure 2 is intended as an initial spectroscopic characterization rather than as a representation of the spectral evolution during electrochemical treatment. Violet S4B is an industrial dye employed in tannery operations rather than a commercially standardized model compound; consequently, information regarding its spectroscopic properties and degradation behavior is scarce. This characterization therefore provides the analytical basis for evaluating the performance of the electrochemical advanced oxidation processes (EAOPs) investigated in this study.

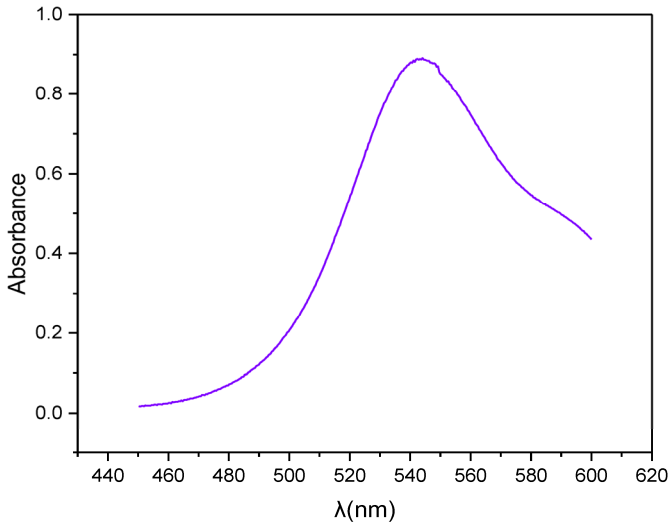


Figure 2. Initial UV–Vis absorption spectrum of 50 mg L^{-1} Violet S4B in 50 mM Na_2SO_4 at pH 3.0, recorded prior to electrochemical treatment for determination of the maximum absorption wavelength (λ_{max}).

As shown in Figure 2, the spectrum exhibits a broad absorption band centered at approximately 541 nm, responsible for the characteristic violet color of the solution. This band is consistent with $\pi \rightarrow \pi^*$ electronic transitions within conjugated aromatic structures typical of industrial dyes designed for high color intensity and chemical stability. The slight asymmetry and broad tail extending toward longer wavelengths suggest the presence of multiple chromophoric groups or substituents that influence the electronic distribution of the molecule.

It should be emphasized that dye discoloration does not necessarily indicate complete mineralization, since chromophore destruction may occur while oxidation intermediates remain in solution [29]. Therefore, UV–Vis analysis was used to monitor color removal, whereas mineralization was evaluated independently by chemical oxygen demand (COD) measurements.

3.2. Electrochemical Characterization of the Dye

The electrochemical behavior of Violet S4B was investigated by cyclic voltammetry to elucidate its redox properties and susceptibility to electrochemical oxidation. Measurements were performed using a potentiostat/galvanostat (BASi) in a conventional three-electrode cell equipped with a glassy carbon working electrode, a platinum wire counter

electrode, and an Ag/AgCl reference electrode. The supporting electrolyte consisted of 50 mM Na_2SO_4 at pH 3.0 containing 50 mg L^{-1} of the dye.

As shown in Figure 3a, the cyclic voltammogram recorded at a scan rate of 100 mV s^{-1} exhibits a single well-defined anodic peak centered at approximately 0.98 V. No corresponding cathodic peak is observed during the reverse scan, indicating that the oxidation process is electrochemically irreversible under the experimental conditions. Such behavior is characteristic of the oxidative transformation of complex aromatic structures, where the primary electron transfer is followed by rapid chemical reactions that prevent regeneration of the parent molecule [30].

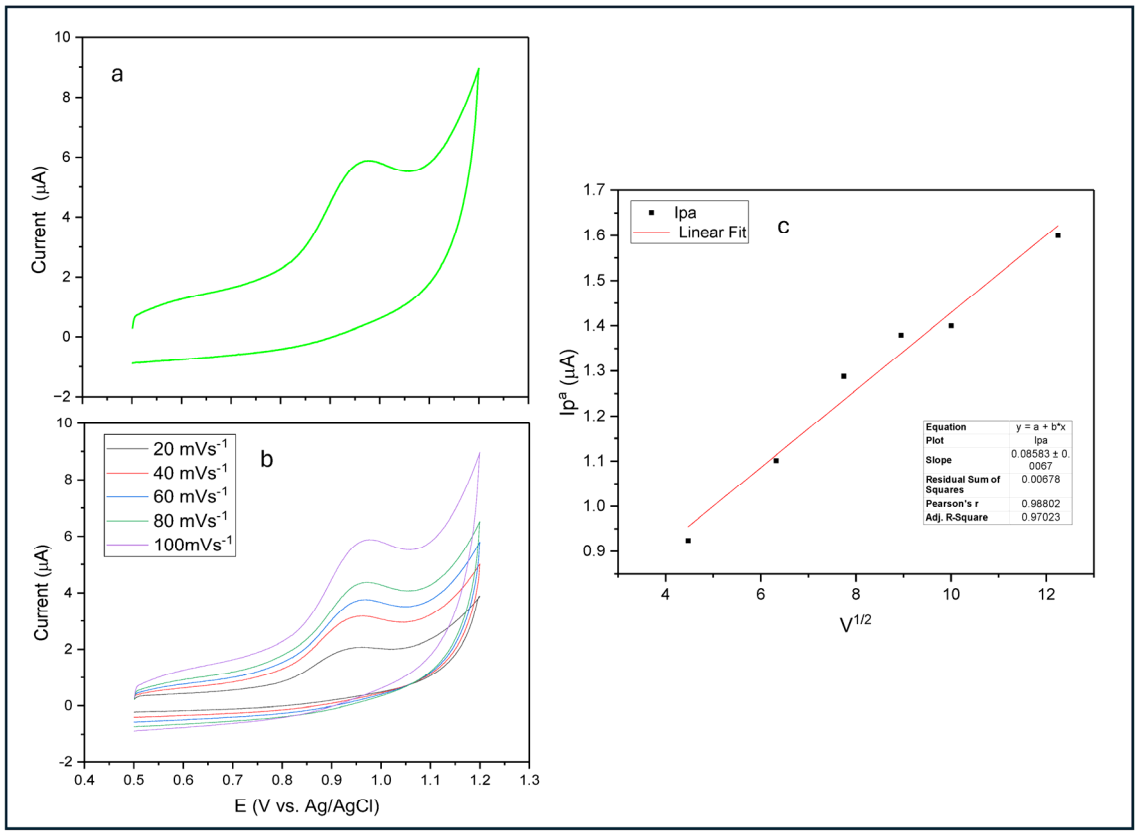


Figure 3. Electrochemical characterization of 50 mg L^{-1} Violet S4B in 50 mM Na_2SO_4: (**a**) cyclic voltammogram at 100 mV s^{-1}, (**b**) cyclic voltammograms at different scan rates, and (**c**) relationship between anodic peak current and the square root of scan rate.

Figure 3b presents the voltammograms recorded at different scan rates, showing a progressive increase in anodic peak current with increasing scan rate. As illustrated in Figure 3c, the anodic peak current (Ipa) varies linearly with the square root of the scan rate, confirming that the oxidation process is predominantly diffusion-controlled. The inset summarizes the regression parameters used to validate the linear relationship. The absence of a reduction peak further indicates that the oxidation products are electrochemically unstable and undergo subsequent homogeneous reactions leading to irreversible degradation of the chromophoric structure. This behavior is consistent with an EC-type mechanism, in which the initial electron transfer is followed by fast chemical transformations in solution [31].

Only minor changes in the anodic peak potential were observed as the scan rate increased, suggesting that the oxidation mechanism remains essentially unchanged within the investigated range. The increase in current can therefore be attributed mainly to enhanced mass transport resulting from a thinner diffusion layer at higher scan rates [32]. During prolonged electrochemical measurements, however, gradual electrode passivation

was observed, most likely due to the accumulation of strongly adsorbed oxidation products or polymeric species on the electrode surface. Consequently, cyclic voltammetry was unsuitable for quantitative determination of Violet S4B because progressive surface fouling reduced the effective electroactive area and compromised calibration reproducibility [33].

Overall, the electrochemical characterization demonstrates that Violet S4B undergoes irreversible anodic oxidation through a diffusion-controlled process. These findings confirm the intrinsic electrochemical reactivity of the dye and provide a mechanistic basis for its subsequent degradation by electrochemical advanced oxidation processes (EAOPs) [34].

3.3. FTIR Characterization of Violet S4B

The FTIR spectrum presented in Figure 4 provides structural information on Violet S4B and its potential influence on the electrochemical oxidation process. The identified absorption bands confirm the predominance of highly conjugated aromatic structures and amine-containing functional groups, which are characteristic of triphenylmethane dyes and are closely related to their chromophoric properties and electrochemical reactivity.

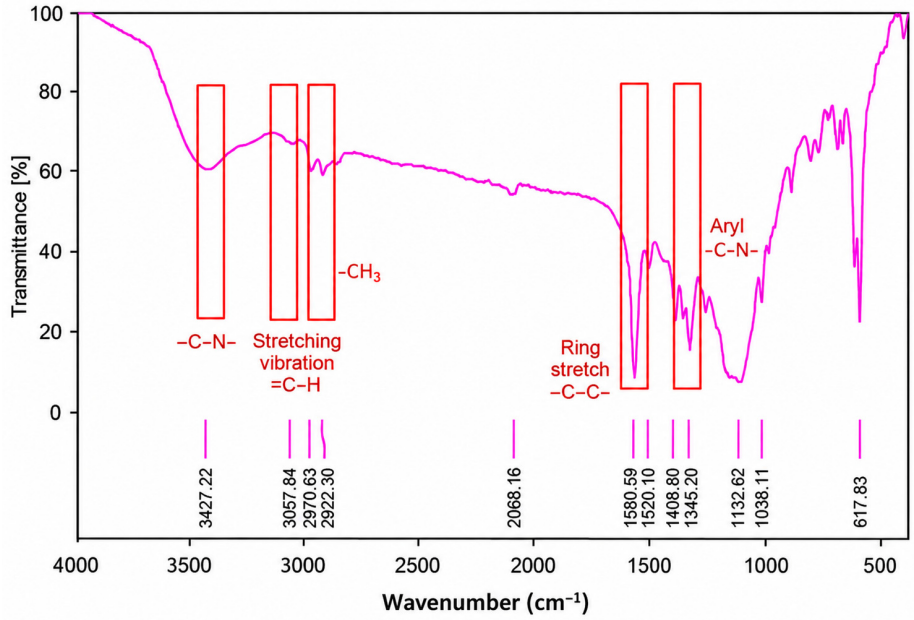


Figure 4. FTIR spectrum of Violet S4B (Crystal Violet).

As shown in Figure 4, a broad absorption band centered at approximately 617 cm^{-1} was observed within the fingerprint region, suggesting the presence of additional structural components associated with the industrial-grade formulation of the dye. Such compositional complexity may influence both the spectroscopic response and the oxidation pathways, particularly during the formation of intermediate species throughout the degradation process [35].

The predominance of aromatic amine groups and extended π-conjugated structures is consistent with the irreversible oxidation behavior observed in the cyclic voltammetry studies, since these functionalities are highly susceptible to oxidative transformation [2]. Likewise, the presence of additional constituents may contribute to electrode fouling through the formation of polymeric or strongly adsorbed oxidation products, which progressively block active sites and decrease the electroactive surface during prolonged electrochemical operation [36].

3.4. Electrochemical Advanced Oxidation Processes

The degradation of Violet S4B by electrochemical oxidation (EOx) was evaluated at initial dye concentrations of 50, 100, and 150 mg L^{-1}, selected to represent the concentration range investigated in this study. Dye concentration was monitored by UV–Vis spectroscopy using a calibration curve constructed from the maximum absorption wavelength (541 nm). The removal efficiency was calculated according to Equation (7):

$$\text{Percent of removal} = (C_0 - C_t)/C_0 \times 100 \quad (7)$$

where C_0 and C_t correspond to the concentration at the initial time and at time t, respectively [37].

3.4.1. Effect of Applied Current Density at Different Initial Concentrations in Electrochemical Oxidation

The electrochemical oxidation (EOx) of Violet S4B was evaluated at current densities of (■) 20 mA cm^{-2}, (●) 50 mA cm^{-2}, and (▲) 70 mA cm^{-2}, using initial dye concentrations of 50, 100, and 150 mg L^{-1} in 50 mM Na_2SO_4 at pH 3.0. Under all experimental conditions, the degradation profiles were satisfactorily described by pseudo-first-order kinetics.

At an initial concentration of 50 mg L^{-1}, Figure 5a shows rapid dye removal, reaching (■) 94.8%, (●) 99.7%, and (▲) 99.9% after 60 min. The corresponding apparent rate constants (Figure 5b) increased from (■) 0.0742 min^{-1} to (●) 0.1505 min^{-1} and (▲) 0.2736 min^{-1} as the current density increased, indicating that the degradation rate was primarily governed by the generation of oxidizing species at the anode [38].

Increasing the initial concentration to 100 mg L^{-1} resulted in lower degradation efficiencies (Figure 5c), with removals of (■) 26.8%, (●) 62.3%, and (▲) 82.3% at 20, 50, and 70 mA cm^{-2}, respectively. Likewise, the apparent rate constants (Figure 5d) decreased to (■) 0.0052 min^{-1}, (●) 0.0162 min^{-1}, and (▲) 0.0298 min^{-1}, reflecting the greater competition for reactive species and the progressive limitation imposed by the higher pollutant load [38].

A similar trend was observed at 150 mg L^{-1}. As shown in Figure 5e, dye removals of (■) 71.6%, (●) 77.8%, and (▲) 81.0% were achieved after 60 min, while the corresponding kinetic constants (Figure 5f) were (■) 0.0210 min^{-1}, (●) 0.0251 min^{-1}, and (▲) 0.0277 min^{-1}. Despite the higher organic loading, the electrochemical process maintained high removal efficiencies over the investigated current density range, demonstrating its suitability for treating concentrated dye solutions.

The improvement in degradation performance with increasing current density is attributed to the enhanced electrogeneration of physisorbed BDD($^{\bullet}$OH) on the anode surface, which increases the oxidation capacity of the system. At the highest current densities, however, part of the applied current may be consumed by competing reactions, particularly oxygen evolution, leading to a partial decrease in current efficiency. Nevertheless, the overall oxidation performance remained high throughout the investigated operating conditions [39].

From a mechanistic standpoint, EOx is dominated by heterogeneous oxidation mediated by BDD($^{\bullet}$OH) generated at the electrode surface. As electrolysis proceeds, the process gradually shifts from reaction-controlled to mass transfer-controlled conditions, making pollutant transport from the bulk solution to the electrode increasingly important. This effect becomes more pronounced at higher dye concentrations, explaining the lower apparent degradation rates despite the higher production of oxidizing species [40].

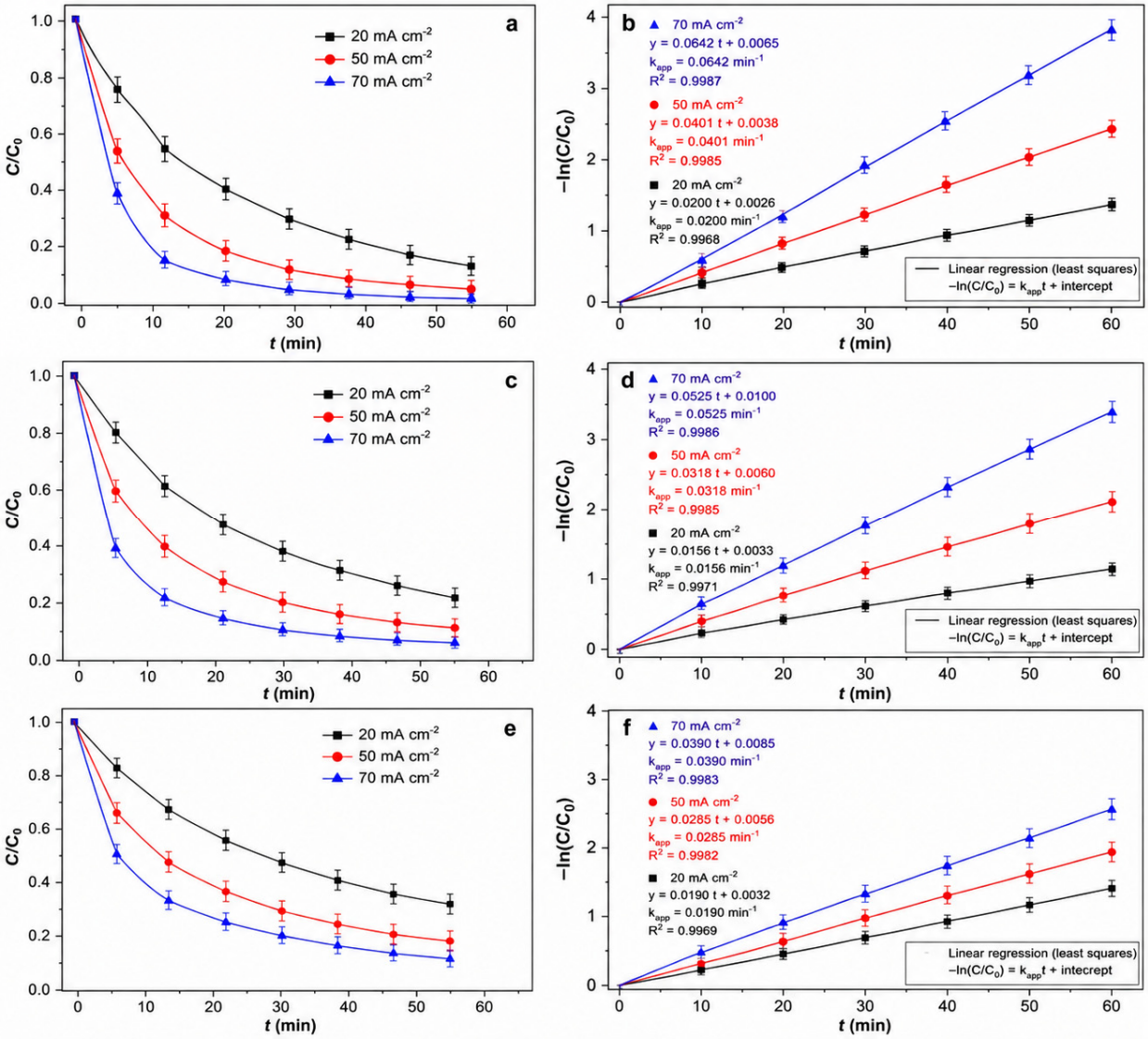


Figure 5. Effect of current density on the electrochemical oxidation of Violet S4B using a BDD anode in 50 mM Na_2SO_4 at pH 3.0 at different initial dye concentrations: (**a**,**b**) 50 mg L^{-1}, (**c**,**d**) 100 mg L^{-1}, and (**e**,**f**) 150 mg L^{-1}. Panels (**a**,**c**,**e**) show the normalized concentration (C/C_0) as a function of electrolysis time, whereas panels (**b**,**d**,**f**) show the corresponding pseudo-first-order kinetic plots, $-\ln(C/C_0)$ versus time, with linear regression fits. The apparent rate constants (kapp) and coefficients of determination (R^2) obtained from the linear regressions are indicated in the kinetic panels. (■) j = 20 mA cm^{-2}, (●) j = 50 mA cm^{-2}, and (▲) j = 70 mA cm^{-2}.

3.4.2. Effect of Initial Concentration in Electrochemical Oxidation

The influence of the initial dye concentration on the performance of the EOx process is presented in Figure 6a. An inverse relationship between the initial concentration and degradation efficiency was observed. At 50 mg L^{-1} (▲), rapid oxidation led to nearly complete dye removal within the early stages of electrolysis. In contrast, increasing the concentration to 100 mg L^{-1} (■) and 150 mg L^{-1} (●) at 70 mA cm^{-2} resulted in progressively slower degradation profiles, reflecting the greater oxidant demand imposed by higher pollutant loadings [41].

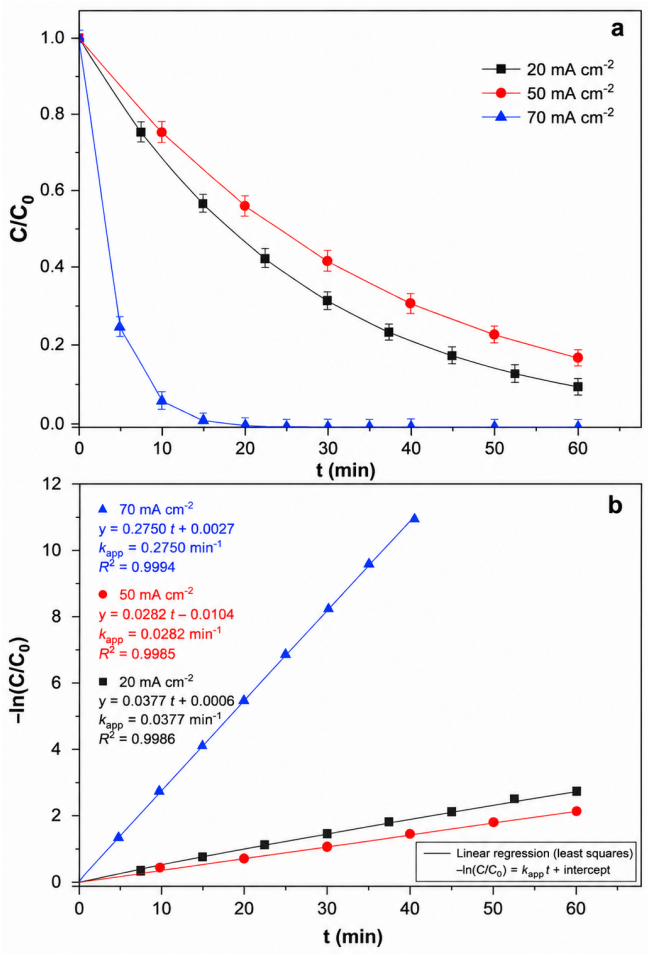


Figure 6. Effect of initial dye concentration on the electrochemical oxidation of Violet S4B at 70 mA cm^{-2} in 50 mM Na_2SO_4 at pH 3.0: (**a**) normalized concentration (C/C_0) as a function of electrolysis time and (**b**) corresponding pseudo-first-order kinetic plots, $-\ln(C/C_0)$ versus time, with linear regression fits. The apparent rate constants (kapp) and coefficients of determination (R^2) obtained from the linear regressions are indicated in panel (**b**). (▲) 50 mg L^{-1}, (■) 100 mg L^{-1}, and (●) 150 mg L^{-1}.

This trend is confirmed by the kinetic analysis shown in Figure 6b, where the apparent rate constants decreased markedly with increasing dye concentration. The system containing 50 mg L^{-1} exhibited the highest apparent rate constant (0.27236 min^{-1}), whereas substantially lower values of 0.0298 min^{-1} and 0.0251 min^{-1} were obtained at 100 and 150 mg L^{-1}, respectively. Overall, increasing the dye concentration from 50 to 150 mg L^{-1} reduced the apparent reaction rate by approximately one order of magnitude [42].

The decrease in degradation kinetics can be attributed primarily to the lower oxidant-to-pollutant ratio as the dye concentration increases. Although the electrogeneration rate of BDD(•OH) remains governed by the applied current, a larger number of dye molecules compete for the same population of reactive species, reducing the probability of effective oxidation events [43]. Simultaneously, oxidation intermediates formed during electrolysis accumulate to a greater extent at higher pollutant concentrations and compete with the parent dye for hydroxyl radicals, further decreasing the overall degradation rate and increasing the complexity of the oxidation pathway [44].

In addition to these chemical effects, mass transport becomes increasingly important at higher dye concentrations. As the oxidation rate at the electrode surface increases, the transport of pollutant molecules from the bulk solution to the electrode may become the limiting step, resulting in lower apparent kinetic constants despite the high oxidation capability of the BDD anode [45].

Overall, these results demonstrate that the efficiency of electrochemical oxidation is strongly dependent on the initial pollutant loading. Lower dye concentrations favor faster degradation because the oxidizing species generated through Equation (1) are more readily available for reaction with the target pollutant, whereas higher concentrations progressively shift the process toward oxidant-limited and mass transfer-controlled conditions.

3.4.3. Effect of Current Density on the Electro-Fenton Process

An initial dye concentration of 150 mg L^{-1} was selected for the electro-Fenton (EF) experiments based on the results obtained during electrochemical oxidation, where satisfactory degradation performance was achieved under comparable operating conditions. Moreover, this concentration is representative of highly contaminated tannery wastewaters, providing a more realistic basis for evaluating the treatment efficiency under practical conditions.

Figure 7a illustrates the degradation of Violet S4B during EF treatment at current densities of (■) 20, (●) 50, and (▲) 70 mA cm^{-2} in 50 mM Na_2SO_4 (pH 3.0) containing 0.02 mM Fe^{2+}. The normalized concentration (C/C_0) decreased more rapidly as the applied current density increased. After 60 min of electrolysis, dye removals of (■) 55%, (●) 78%, and (▲) 96% were achieved at 20, 50, and 70 mA cm^{-2}, respectively. This behavior reflects the greater electrogeneration of H_2O_2 at higher current densities, which enhances hydroxyl radical production through the Fenton reaction and consequently increases the overall oxidation capacity of the system [46].

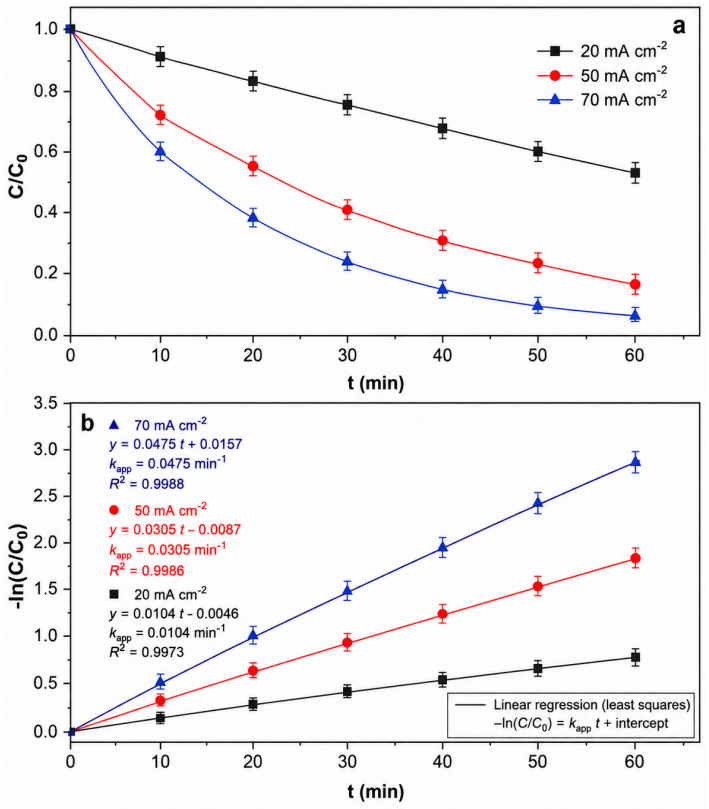


Figure 7. Electro-Fenton degradation of 150 mg L^{-1} Violet S4B using BDD electrodes in 50 mM Na_2SO_4 at pH 3.0 with 0.02 mM Fe^{2+}: (**a**) normalized concentration (C/C_0) as a function of electrolysis time at different current densities and (**b**) corresponding pseudo-first-order kinetic plots, $-\ln(C/C_0)$ versus time, with linear regression fits. The apparent rate constants (k_{app}) and coefficients of determination (R^2) obtained from the linear regressions are indicated in panel (**b**). (■) 20 mA cm^{-2}, (●) 50 mA cm^{-2}, and (▲) 70 mA cm^{-2}.

The kinetic analysis presented in Figure 7b confirms that dye degradation follows pseudo-first-order kinetics over the investigated current density range. The apparent rate constants increased from (■) 0.0104 min^{-1} to (●) 0.0305 min^{-1} and (▲) 0.0475 min^{-1} as the current density increased, demonstrating that the degradation rate is strongly governed by the availability of reactive oxygen species generated during the EF process [47].

From a mechanistic perspective, increasing the applied current enhances the cathodic reduction of dissolved oxygen to H_2O_2, which subsequently reacts with Fe^{2+} to generate hydroxyl radicals in the bulk solution. This homogeneous oxidation pathway complements the heterogeneous oxidation occurring at the BDD anode, producing a synergistic effect that accelerates dye degradation. Nevertheless, excessively high current densities may also promote competing reactions, such as hydrogen evolution at the cathode and oxygen evolution at the anode, which can partially reduce current efficiency despite the higher oxidation rate.

Overall, the EF process exhibited a pronounced dependence on current density, with higher applied currents producing faster degradation kinetics and greater discoloration efficiencies. These results demonstrate the superior oxidation capability of EF compared with direct electrochemical oxidation under equivalent pollutant loading and support its applicability for the treatment of highly concentrated tannery dye solutions [48].

3.4.4. Photoelectro-Fenton Process

Figure 8a presents the degradation of 150 mg L^{-1} Violet S4B by the photoelectro-Fenton (PEF) process in 50 mM Na_2SO_4 at pH 3.0 using current densities of (■) 20, (●) 50, and (▲) 70 mA cm^{-2}. As observed for EOx and EF, increasing the applied current density significantly enhanced the degradation performance owing to the greater production of reactive oxygen species. Dye removals after 60 min reached (■) 92%, (●) 98%, and (▲) complete discoloration at 20, 50, and 70 mA cm^{-2}, respectively. The corresponding pseudo-first-order kinetic constants (Figure 8b) increased from (■) 0.0466 min^{-1} to (●) 0.0733 min^{-1} and (▲) 0.0992 min^{-1}, confirming the acceleration of the oxidation process with increasing current density. Based on these results, 70 mA cm^{-2} was selected for the subsequent evaluation of the effect of the initial dye concentration [49].

The influence of the initial pollutant loading is shown in Figure 9. Complete dye removal was achieved after (■) 35 min for 50 mg L^{-1}, (●) 50 min for 100 mg L^{-1}, and (▲) 60 min for 150 mg L^{-1} under identical operating conditions. Although higher dye concentrations increased the treatment time, the PEF process maintained excellent degradation performance throughout the investigated concentration range, demonstrating its robustness under variable organic loads [50].

A comparative assessment of the three electrochemical processes is presented in Figure 10a. Under the specific electrode configurations and operating conditions employed for each process, the degradation performance followed the order ▲ PEF > ● EF > ■ EOx. However, this comparison should not be interpreted as a strictly controlled evaluation of the intrinsic contribution of Fenton chemistry and UV irradiation alone, since the electrode configuration differed between treatments: EOx employed a BDD anode coupled with a stainless-steel cathode, whereas EF and PEF employed BDD electrodes as both anode and cathode. Therefore, the observed differences reflect the overall performance of each experimental configuration, including both the oxidation mechanism and the electrode arrangement. Within this context, the enhanced performance observed for EF and particularly PEF is consistent with the additional contribution of electrogenerated H_2O_2 and homogeneous Fenton chemistry, while UV irradiation in PEF further promotes Fe^{3+} photoreduction and the photolysis of Fe(III)-carboxylate complexes, enhancing the availability of reactive oxidizing species [51].

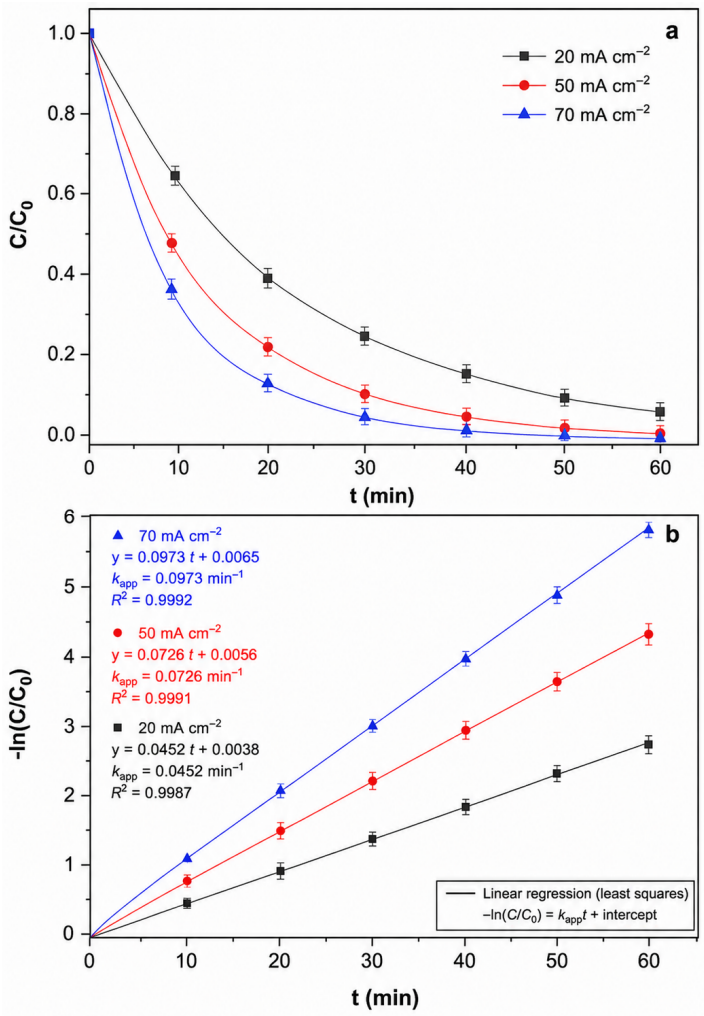


Figure 8. Photoelectro-Fenton degradation of 150 mg L^{-1} Violet S4B using BDD electrodes in 50 mM Na_2SO_4 at pH 3.0: (**a**) normalized concentration (C/C_0) as a function of electrolysis time at different current densities and (**b**) corresponding pseudo-first-order kinetic plots, $-\ln(C/C_0)$ versus time, with linear regression fits. The apparent rate constants (k_{app}) and coefficients of determination (R^2) obtained from the linear regressions are indicated in panel (**b**). (■) 20 mA cm^{-2}, (●) 50 mA cm^{-2}, and (▲) 70 mA cm^{-2}.

The kinetic comparison shown in Figure 10b further demonstrates the superiority of the photo-assisted process. Apparent rate constants of (■) 0.0384 min^{-1}, (●) 0.0470 min^{-1}, and (▲) 0.0992 min^{-1} were obtained for EOx, EF, and PEF, respectively. Notably, PEF achieved more than 95% dye removal within only 30 min, whereas comparable removals required approximately 60 min for both EOx and EF. These results confirm that UV irradiation enhances not only the generation but also the effective utilization of oxidizing species, leading to substantially faster degradation kinetics and improved overall process performance [52,53].

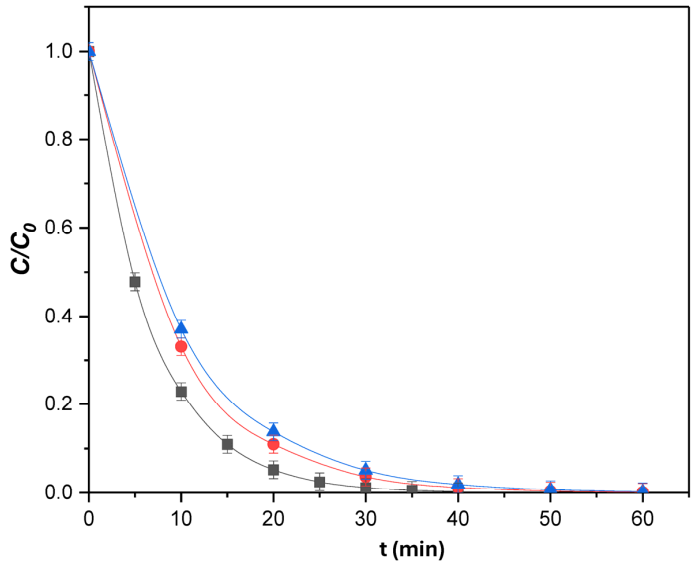


Figure 9. Decay of Violet S4B concentration at different initial dye concentrations (50, 100, and 150 mg L^{-1}) under identical experimental photoelectro-Fenton conditions. Complete removal was achieved after 35 min (■), 50 min (●), and 60 min (▲) for initial concentrations of 50, 100, and 150 mg L^{-1}, respectively.

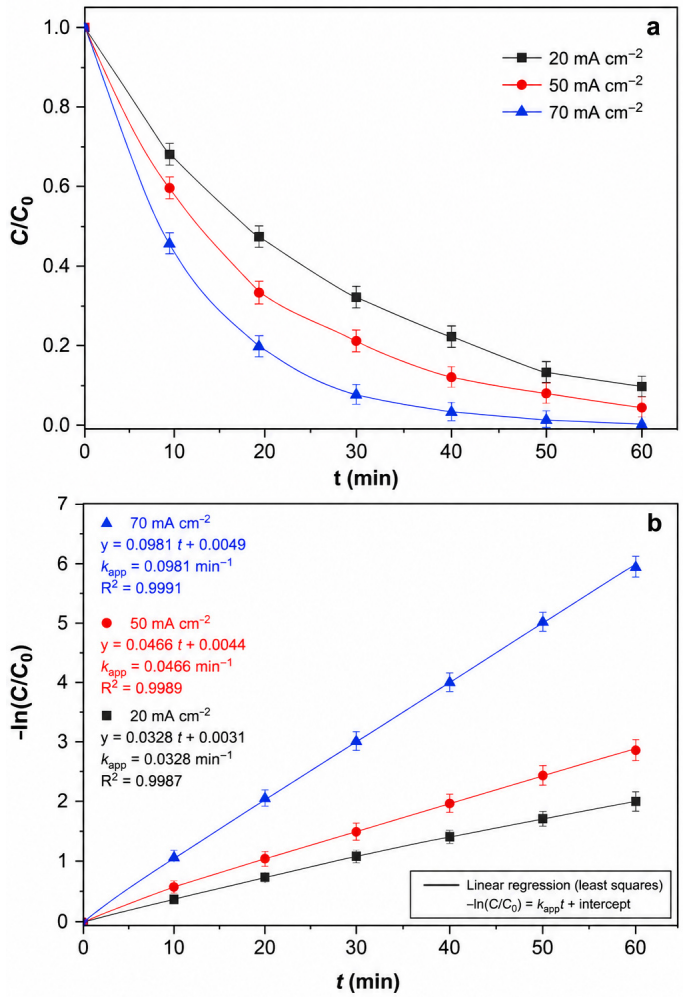


Figure 10. Comparison of electrochemical oxidation (EOx, ■), electro-Fenton (EF, ●) and photoelectro-Fenton (PEF, ▲) processes for the degradation of 150 mg L^{-1} Violet S4B at 70 mA cm^{-2}: (**a**) normalized concentration decay vs. time and (**b**) pseudo-first-order kinetic analysis.

3.4.5. Electrochemical Behavior of Dye Mixtures

Real tannery dye solutions contain complex mixtures of dyes and auxiliary chemicals rather than individual pollutants. Therefore, evaluating electrochemical advanced oxidation processes under multicomponent conditions provides a more realistic assessment of their practical applicability. In this study, a representative dye mixture containing a total concentration of 150 mg L^{-1} was prepared using 50 mg L^{-1} each of Violet S4B, Brown DR, and Black NT2 in 50 mM Na_2SO_4 at pH 3.0. All experiments were performed at 70 mA cm^{-2}, and the discoloration of the ternary dye mixture was monitored from the decrease in absorbance at 514 nm. The wavelength of 514 nm was selected as the monitoring wavelength for the multicomponent system based on the absorption response of the combined dye solution. The absorbance at this wavelength was used as a global spectrophotometric response to follow the degradation of the ternary mixture and was not intended to independently quantify the concentration of each individual dye.

As shown in Figure 11a, all three electrochemical treatments produced a continuous decrease in the normalized dye concentration throughout the treatment period. Under the specific electrode configurations employed in this study, PEF (▲) exhibited the highest discoloration efficiency, achieving approximately 99% after 120 min, followed by EF (●) with nearly 97%, whereas EOx (■) reached approximately 95%. However, these differences should be interpreted as the overall performance of the respective experimental configurations rather than as a strictly controlled comparison of the intrinsic oxidation mechanisms, because EOx employed a BDD anode coupled with a stainless-steel cathode, whereas EF and PEF employed BDD electrodes as both anode and cathode. Thus, the observed performance differences may reflect contributions from both the electrode arrangement and the additional oxidative pathways associated with the Fenton-based processes.

The kinetic analysis presented in Figure 11b further illustrates the differences in degradation rates among the three experimental configurations. The apparent rate constants increased from 0.0259 min^{-1} for EOx to 0.0290 min^{-1} for EF and 0.0321 min^{-1} for PEF. Relative to EOx, these values correspond to increases of approximately 12% and 24% for EF and PEF, respectively. Nevertheless, because the cathode material differed between EOx and the Fenton-based systems, these kinetic differences cannot be attributed exclusively to the incorporation of Fenton chemistry and UV irradiation. Rather, they should be interpreted as reflecting the combined influence of electrode configuration and the additional homogeneous and photo-assisted oxidation pathways operating in EF and PEF [22].

From a mechanistic perspective, the higher degradation rates observed for the Fenton-based configurations are consistent with the contribution of additional oxidation pathways beyond anodically generated BDD($^{\bullet}OH$). In EF, electrogenerated H_2O_2 reacts with Fe^{2+} to produce hydroxyl radicals in the bulk solution, whereas PEF additionally benefits from UV-assisted Fe^{3+} photoreduction and the photolysis of Fe(III)-carboxylate complexes. These mechanisms can enhance the availability and utilization of reactive oxidizing species. However, because the electrode configuration was not identical among all three treatments, the individual contribution of each mechanism cannot be fully isolated from the effect of the electrode arrangement [25,28,30,50].

From an environmental perspective, the experiments performed with the representative multicomponent dye system provide a more relevant assessment of treatment performance than evaluations based exclusively on a single model compound. The simultaneous presence of Violet S4B, Brown DR, and Black NT2 introduces competition among organic constituents for the reactive species generated during treatment, thereby approaching the chemical complexity encountered in dye-containing industrial effluents. Despite this increased complexity, PEF maintained the highest degradation rate and achieved approximately 99% discoloration, demonstrating that the benefits of photo-assisted electrochemical

oxidation are preserved under multicomponent conditions. These findings are particularly relevant for environmental remediation because they indicate that the process can effectively reduce the pollutant load of complex dye mixtures rather than being limited to the degradation of isolated model contaminants. Nevertheless, validation using real tannery dyes containing dyes, dissolved organic matter, inorganic ions, and other auxiliary chemicals will be required to further assess the applicability of the process under actual industrial conditions.

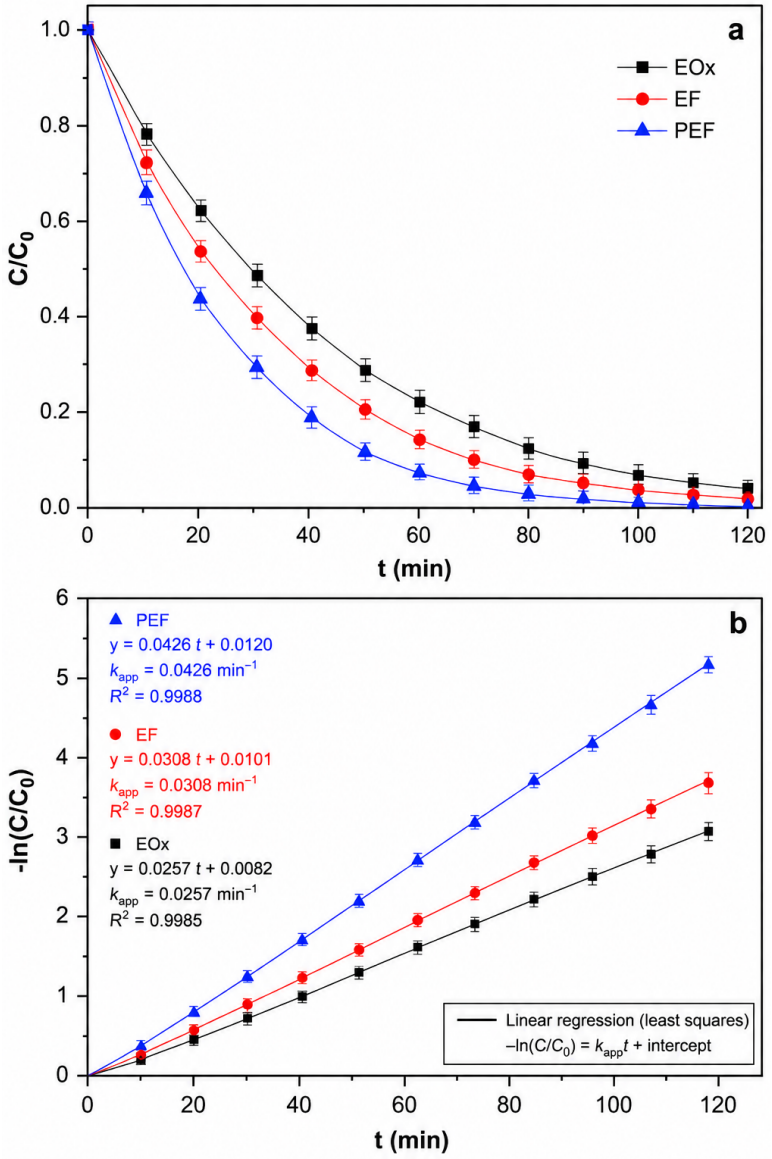


Figure 11. Degradation of a ternary dye mixture (50 mg L^{-1} each of Violet S4B, Brown DR, and Black NT2) using EOx (■), EF (●), and PEF (▲) processes: (**a**) normalized concentration decay vs. time and (**b**) pseudo-first-order kinetic analysis.

3.4.6. Comparative Performance of Electrochemical Oxidation Processes

The comparative evaluation of EOx, EF, and PEF clearly demonstrates the benefits of progressively integrating electrochemical oxidation, Fenton chemistry, and UV irradiation. The incorporation of additional oxidation pathways increased the availability and utilization of reactive oxygen species, resulting in faster degradation kinetics and improved oxidation performance.

For Violet S4B degradation, the apparent pseudo-first-order rate constants increased from 0.0384 min^{-1} for EOx to 0.0470 min^{-1} for EF and 0.0992 min^{-1} for PEF. Relative to

conventional electrochemical oxidation, these values correspond to kinetic enhancement factors of 1.22 and 2.58 for EF and PEF, respectively. Likewise, for the multicomponent dye mixture, the apparent rate constants increased from 0.0259 min^{-1} for EOx to 0.0290 min^{-1} for EF and 0.0321 min^{-1} for PEF, corresponding to enhancement factors of 1.12 and 1.24, respectively. A summary of the kinetic performance of the three oxidation systems is presented in Table 1.

Table 1. Apparent pseudo-first-order rate constants and kinetic enhancement factors for EOx, EF and PEF.

System	Process	kapp (min^{-1})	Intensification Factor
Violet S4B	EOx	0.0384	1.00
Violet S4B	EF	0.0470	1.22
Violet S4B	PEF	0.0992	2.58
Dye mixture	EOx	0.0259	1.00
Dye mixture	EF	0.0290	1.12
Dye mixture	PEF	0.0321	1.24

Intensification Factor = $k_{process}/k_{EOx}$.

Overall, the comparative analysis demonstrates that incorporating homogeneous Fenton chemistry and UV irradiation progressively improves process performance, with PEF consistently providing the highest degradation rates under both single-dye and multicomponent conditions. The results further indicate that these advantages are maintained in representative tannery dye mixtures, supporting the applicability of photo-assisted electrochemical oxidation for the treatment of complex industrial wastewaters and providing useful criteria for selecting electrochemical treatment strategies according to wastewater composition and treatment objectives.

3.4.7. Mineralization Assessment by Chemical Oxygen Demand

From an environmental remediation perspective, discoloration alone is insufficient to demonstrate effective treatment of dye-contaminated wastewater because the destruction of chromophoric groups does not necessarily imply the removal of the associated organic pollutant load. Oxidation intermediates may remain in solution after color disappearance and continue contributing to the chemical oxygen demand of the treated water. Therefore, COD evolution was evaluated together with discoloration during PEF treatment of the multicomponent dye system to distinguish between chromophore destruction and the progressive oxidation of residual organic matter. This combined assessment provides a more environmentally relevant measure of treatment performance by determining whether the process promotes not only rapid color removal but also extensive mineralization of the organic constituents and their transformation products [54].

Figure 12a compares the evolution of (■) dye removal and (■) normalized COD during the treatment of the representative dye mixture. Dye removal proceeded rapidly, reaching approximately 70% within the first 10 min, 90% after 20 min, and exceeding 95% after 30 min, with nearly complete discoloration attained between 40 and 60 min of electrolysis [55].

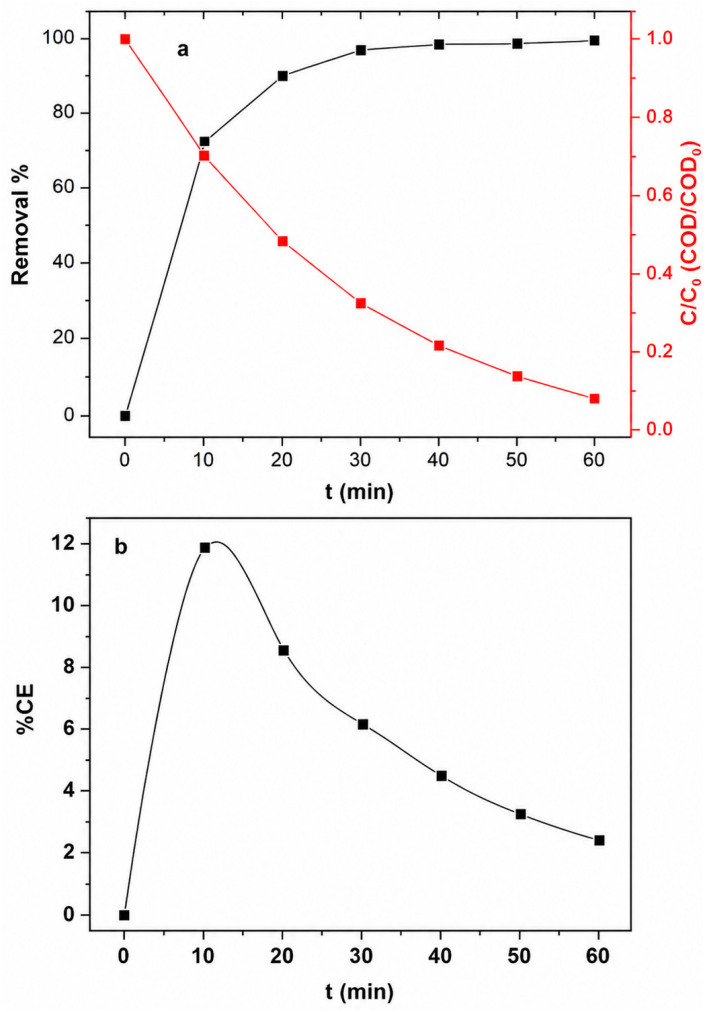


Figure 12. Performance parameters during PEF treatment of the ternary dye mixture: (**a**) percentage of removal and COD decay and (**b**) current efficiency (%CE).

In contrast, COD removal followed a slower and more gradual trend. The normalized COD decreased from an initial value of 1.0 to approximately 0.4 after 10 min, 0.15 after 20 min, 0.05 after 30 min, and approached zero after 50–60 min of treatment. These results indicate that although chromophore destruction occurs rapidly, complete mineralization requires additional oxidation of intermediate species generated during dye degradation, confirming that discoloration alone is not a reliable indicator of complete pollutant removal.

The variation in current efficiency (CE), calculated from the COD data, is presented in Figure 12b. CE progressively decreased from 11.62% at the beginning of the treatment to 2.16% at the end of electrolysis. This behavior reflects the gradual depletion of readily oxidizable organic compounds, which reduces the probability of productive reactions with electrochemically and photochemically generated hydroxyl radicals. As mineralization progresses, oxidation becomes increasingly limited by mass transport and by the persistence of more refractory intermediates, particularly low-molecular-weight carboxylic acids, which react more slowly with •OH. Simultaneously, competing reactions such as oxygen evolution at the BDD anode, hydroxyl radical recombination, and non-productive H_2O_2 decomposition consume part of the applied current, contributing to the observed decline in current efficiency.

Despite this progressive decrease, the continuous photochemical regeneration of Fe^{2+} through the reduction of Fe^{3+} species and the photolysis of Fe(III)-carboxylate complexes sustained the Fenton cycle and enabled almost complete mineralization after prolonged

electrolysis. These results demonstrate that PEF effectively couples rapid discoloration with extensive mineralization, highlighting its potential for treating complex model systems.

3.4.8. HPLC Analysis of Degradation Products in Dye Mixtures

High-performance liquid chromatography (HPLC) was employed to identify degradation products formed during the treatment of the dye mixture, with particular emphasis on low-molecular-weight carboxylic acids, which are recognized as key intermediates during the oxidative degradation of aromatic dyes and useful indicators of the mineralization process.

Figure 13 compares the chromatogram obtained from the final aliquot collected after PEF treatment with that of a 20 mg L^{-1} oxalic acid standard analyzed under identical chromatographic conditions. The standard chromatogram (red) exhibited a well-defined oxalic acid peak with a retention time (Rt) of approximately 6.5 min. In contrast, the chromatogram of the treated sample (blue) displayed only a very weak signal at the same retention time, indicating that oxalic acid did not accumulate significantly during the oxidation process.

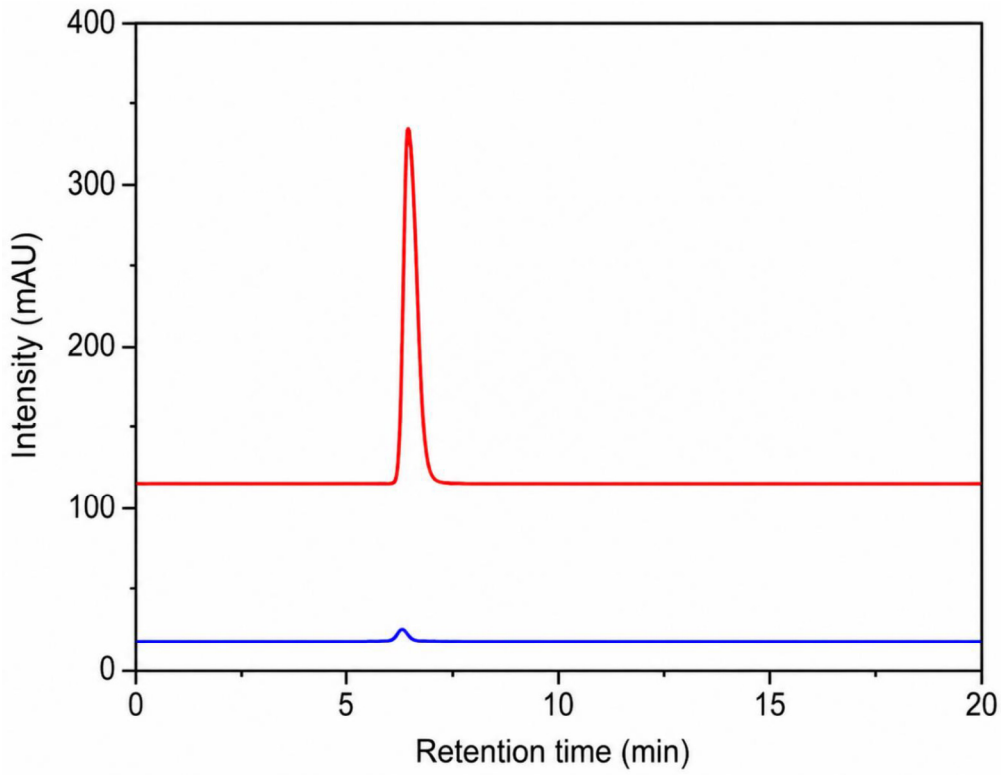


Figure 13. HPLC chromatograms of the final treated dye mixture by PEF (in blue) showing the peak assigned to oxalic acid (R_t = 6.51 min). In red, solution of standard oxalic acid.

This behavior can be attributed to the photo-assisted chemistry occurring during PEF treatment. Oxalic acid forms complexes with Fe(III) that can undergo photolysis under irradiation, as described by Equation (6), simultaneously promoting Fe^{2+} regeneration and further oxidation of the carboxylic intermediate toward CO_2. This pathway contributes to maintaining the Fe^{2+}/Fe^{3+} catalytic cycle while favoring the removal of low-molecular-weight intermediates that may otherwise persist during the final stages of treatment [51,56]. The negligible residual concentration of oxalic acid observed by HPLC is therefore consistent with the substantial COD reduction achieved during PEF treatment and provides complementary evidence of the extensive mineralization promoted by the photo-assisted electrochemical process.

From an environmental remediation perspective, these results are particularly relevant because discoloration alone does not necessarily indicate the removal of the organic pollutant load. Destruction of the chromophoric structures may occur rapidly, while oxidation products can remain in solution and continue contributing to residual organic matter. In this study, the combination of extensive COD removal and negligible accumulation of oxalic acid indicates that PEF treatment proceeds beyond visible dye removal toward the oxidation of low-molecular-weight degradation products. Taken together, the UV–Vis, COD, and HPLC results demonstrate that the photoelectro-Fenton process promotes both effective discoloration and extensive mineralization of the representative multicomponent tannery dye system, strengthening its potential as an environmental remediation strategy for complex dye-contaminated wastewaters [51,56].

4. Conclusions

This study demonstrates the potential of electrochemical advanced oxidation processes for the remediation of tannery dye-contaminated water through a comparative evaluation of electrochemical oxidation (EOx), electro-Fenton (EF), and photoelectro-Fenton (PEF) using BDD electrodes. The progressive integration of anodic oxidation, homogeneous Fenton chemistry, and UV-assisted reactions enhanced pollutant degradation and mineralization, with treatment performance consistently following the order EOx < EF < PEF for both Violet S4B and the representative multicomponent dye mixture.

The evaluation of the multicomponent system provided a more environmentally relevant assessment of treatment performance than experiments based exclusively on a single dye, since the simultaneous presence of Violet S4B, Brown DR, and Black NT2 introduced competition for the reactive species generated during oxidation. Despite this increased complexity, PEF maintained the highest degradation rate and achieved approximately 99% discoloration, demonstrating the robustness of the photo-assisted process under conditions approaching the complexity of dye-containing industrial effluents.

The combined UV–Vis, COD, and HPLC analyses further demonstrated that rapid discoloration should not be considered equivalent to complete removal of the organic pollutant load. Although chromophore destruction occurred rapidly, additional treatment was required for the oxidation of the resulting intermediates. The extensive COD removal achieved by PEF, together with the negligible accumulation of oxalic acid at the end of treatment, confirmed that the process proceeded beyond visible color removal toward extensive oxidation and mineralization of residual organic matter.

Overall, the superior kinetic performance, extensive mineralization, and effectiveness of BDD-based PEF under multicomponent conditions highlight its potential as an environmental remediation strategy for persistent organic pollution associated with tannery effluents. These findings support the application of EAOPs to complex dye-contaminated waters while emphasizing the importance of evaluating treatment performance through both pollutant degradation and mineralization. Further validation using real multicomponent dye mixtures and larger-scale treatment systems will be necessary to determine process performance in the presence of the broader chemical complexity encountered under actual industrial conditions.

Author Contributions: Investigation and writing—original draft preparation, Y.G.L.-D.; writing—review and editing, Y.G.L.-D.; methodology and writing—review and editing, M.O.A.P.-Á.; writing—review and editing, S.G.-G.; writing—review and editing, O.S.; writing—review and editing, P.E.; writing—review and editing, E.B.; writing—original draft preparation, writing—review and editing, and project administration, J.M.P.-H. All authors have read and agreed to the published version of the manuscript.

Funding: This research was funded by Universidad de Guanajuato, grant number CIIC-UG 188/2026, and by Laboratorio Nacional CONAHCYT de Ciencia y Tecnología del Agua (LNCyTA), grant number LN-2025-I-16.

Data Availability Statement: The original contributions presented in this study are included in the article. Further inquiries can be directed to the corresponding author.

Conflicts of Interest: The authors declare no conflicts of interest.

References

1. Zhao, J.; Wu, Q.; Tang, Y.; Zhou, J.; Guo, H. Tannery wastewater treatment: Conventional and promising processes, an updated 20-year review. *J. Leather Sci. Eng.* **2022**, *4*, 10. [CrossRef]
2. Bhardwaj, A.; Kumar, S.; Singh, D. Tannery effluent treatment and its environmental impact: A review of current practices and emerging technologies. *Water Qual. Res. J.* **2023**, *58*, 128–152. [CrossRef]
3. Yusuf, F.G.; Rasheed, A.A.; Ibrahim, A.B.; Ogunleye, S. Energy and resource recovery from tannery wastewater for sustainable leather production. *Discov. Environ.* **2026**, *4*, 39. [CrossRef]
4. Lin, J.; Ye, W.; Xie, M.; Seo, D.H.; Luo, J.; Wan, Y.; Van der Bruggen, B. Environmental impacts and remediation of dye-containing wastewater. *Nat. Rev. Earth Environ.* **2023**, *4*, 785–803. [CrossRef]
5. Tkaczyk-Wlizło, A.; Mitrowska, K. The occurrence of pharmacologically active dyes in the aquatic environment as a result of water and wastewater contamination—An underestimated environmental problem. *Environ. Sci. Pollut. Res.* **2026**, *33*, 9225–9255. [CrossRef] [PubMed]
6. Patel, D.; Singh, A.; Ambati, S.R.; Singh, R.S.; Sonwani, R.K. An overview of recent advances in treatment of complex dye-containing wastewater and its techno-economic assessment. *J. Environ. Manag.* **2024**, *370*, 122804. [CrossRef] [PubMed]
7. *NOM-001-SEMARNAT-2021*; Norma Oficial Mexicana NOM-001-SEMARNAT-2021, Que Establece los Límites Permisibles de Contaminantes en las Descargas de Aguas Residuales en Cuerpos Receptores Propiedad de la Nación. Diario Oficial de la Federación: Mexico City, Mexico, 2022.
8. Yaseen, D.A.; Scholz, M. Textile dye wastewater characteristics and constituents of synthetic effluents: A critical review. *Int. J. Environ. Sci. Technol.* **2019**, *16*, 1193–1226. [CrossRef]
9. Matesun, J.; Petrik, L.; Musvoto, E.; Ayinde, W.; Ikumi, D. Limitations of wastewater treatment plants in removing trace anthropogenic biomarkers and future directions: A review. *Ecotoxicol. Environ. Saf.* **2024**, *281*, 116610. [CrossRef] [PubMed]
10. Bashir, Y.; Raj, R.; Ghangrekar, M.M.; Nema, A.K.; Das, S. Critical assessment of advanced oxidation processes and bio-electrochemical integrated systems for removing emerging contaminants from wastewater. *RSC Sustain.* **2023**, *1*, 1912–1931. [CrossRef]
11. Zhang, S.; Zheng, H.; Tratnyek, P.G. Advanced redox processes for sustainable water treatment. *Nat. Water* **2023**, *1*, 666–681. [CrossRef]
12. Ganiyu, S.O.; Martínez-Huitle, C.A.; Oturan, M.A. Electrochemical advanced oxidation processes for wastewater treatment: Advances in formation and detection of reactive species and mechanisms. *Curr. Opin. Electrochem.* **2021**, *27*, 100678. [CrossRef]
13. Martínez-Huitle, C.A.; Panizza, M. Electrochemical oxidation of organic pollutants for wastewater treatment. *Curr. Opin. Electrochem.* **2018**, *11*, 62–71. [CrossRef]
14. Asaithambi, P.; Yesuf, M.B.; Govindarajan, R.; Hariharan, N.; Thangavelu, P.; Alemayehu, E. A Review of Hybrid Process Development Based on Electrochemical and Advanced Oxidation Processes for the Treatment of Industrial Wastewater. *Int. J. Chem. Eng.* **2022**, *2022*, 1105376. [CrossRef]
15. Deng, F.; Jiang, J.; Sirés, I. State-of-the-art review and bibliometric analysis on electro-Fenton process. *Carbon Lett.* **2023**, *33*, 17–34. [CrossRef] [PubMed]
16. Nidheesh, P.V.; Trellu, C.; Vargas, H.O.; Mousset, E.; Ganiyu, S.O.; Oturan, M.A. Electro-Fenton process in combination with other advanced oxidation processes: Challenges and opportunities. *Curr. Opin. Electrochem.* **2023**, *37*, 101171. [CrossRef]
17. Chen, M.; Chen, J.P. Achieving cycling catalysis of electro-Fenton treatment. *Nat. Water* **2024**, *2*, 702–703. [CrossRef]
18. Olvera-Vargas, H.; Trellu, C.; Nidheesh, P.V.; Mousset, E.; Ganiyu, S.O.; Martínez-Huitle, C.A.; Zhou, M.; Oturan, M.A. Challenges and opportunities for large-scale applications of the electro-Fenton process. *Water Res.* **2024**, *266*, 122430. [CrossRef] [PubMed]
19. McBeath, S.T.; Mora, A.S.; Zeidabadi, F.A.; Mayer, B.K.; McNamara, P.; Mohseni, M.; Hoffmann, M.R.; Graham, N.J. Progress and prospect of anodic oxidation for the remediation of perfluoroalkyl and polyfluoroalkyl substances in water and wastewater using diamond electrodes. *Curr. Opin. Electrochem.* **2021**, *30*, 100865. [CrossRef]
20. Brillas, E.; Peralta-Hernandez, J.M. The recent development of innovative photoelectro-Fenton processes for the effective and cost-effective remediation of organic pollutants in waters. *Chemosphere* **2024**, *366*, 143465. [CrossRef] [PubMed]
21. Chen, X.; Wang, Y.; Fan, X.; Zhu, G.; Liu, Y.; Quan, X. Efficient electro-Fenton degradation of organic pollutants via the synergistic effect of $^1O_2$ and •OH generated on single Fe–N4 sites. *Sci. Total Environ.* **2024**, *932*, 173042. [CrossRef] [PubMed]

22. Zhang, L.; Peng, W.; Wang, W.; Cao, Y.; Fan, G.; Huang, Y.; Qi, M. A comprehensive review of the electrochemical advanced oxidation processes: Detection of free radical, electrode materials and application. *J. Environ. Chem. Eng.* **2024**, *12*, 113778. [CrossRef]
23. Trench, A.B.; Oturan, N.; Demir, A.; Moura, J.P.; Trellu, C.; Santos, M.C.; Oturan, M.A. Degradation of methylparaben by anodic oxidation, electro-Fenton, and photoelectro-Fenton using carbon felt-BDD cell. *Sep. Purif. Technol.* **2025**, *371*, 133335. [CrossRef]
24. Bravo-Yumi, N.; Pacheco-Álvarez, M.O.; Olvera-Vargas, H.; Brillas, E.; Peralta-Hernández, J.M. Electrochemical treatment on a pilot scale of a mixture with high concentrations of dyes from the tanning/textile industry. *J. Electroanal. Chem.* **2024**, *972*, 118616. [CrossRef]
25. Razzaq, U.; Nguyen, T.-B.; Saleem, M.U.; Le, V.-R.; Chen, C.-W.; Bui, X.-T.; Dong, C.-D. Recent progress in electro-Fenton technology for the remediation of pharmaceutical compounds in aqueous environments. *Sci. Total Environ.* **2024**, *946*, 174253. [CrossRef] [PubMed]
26. Barcenas-Grangeno, C.; Pacheco-Álvarez, M.O.A.; Brillas, E.; Sandoval, M.A.; Peralta-Hernández, J.M. Kinetic insights and process selection for electrochemical remediation of industrial dye effluents using mixed electrode systems. *Processes* **2025**, *13*, 3439. [CrossRef]
27. Herrera-Chávez, S.; Gutierrez, S.; Sandoval, M.A.; Brillas, E.; Pacheco-Álvarez, M.; Peralta-Hernández, J.M. Sustainable degradation of acetaminophen by a solar-powered electro-fenton process. *Processes* **2025**, *13*, 2633. [CrossRef]
28. Gadi, N.; de Souza, A.B.; Boelee, N.C.; Cabooter, D.; Dewil, R. Elimination of miconazole nitrate from water by electro-Fenton: Effect of operating parameters and degradation pathway. *Environ. Sci. Water Res. Technol.* **2025**, *11*, 1898–1908. [CrossRef]
29. Schroeder, C.M.; Koehler, T.M.; Ohlhorst, K.K.; Leadbeater, N.E. Real-time in situ monitoring using visible spectrophotometry as a tool for probing electrochemical advanced oxidation processes for dye decolorisation. *RSC Adv.* **2023**, *13*, 33559–33565. [CrossRef] [PubMed]
30. Lei, X.; Hu, S.; Liu, K.; Lv, X.; Chen, Y.; Zhang, Q.; Jia, Y.; Zhong, K.; Wang, B.; Xu, T. Electrochemical oxidation of Rhodamine B in dye wastewater by a novel boron-doped diamond electrode: Parameter optimization and degradation mechanism. *Desalin. Water Treat.* **2024**, *317*, 100243. [CrossRef]
31. He, Y.; Lin, H.; Guo, Z.; Zhang, W.; Li, H.; Huang, W. Recent developments and advances in boron-doped diamond electrodes for electrochemical oxidation of organic pollutants. *Sep. Purif. Technol.* **2019**, *212*, 802–821. [CrossRef]
32. Kislyi, A.; Moroz, I.; Guliaeva, V.; Prokhorov, Y.; Klevtsova, A.; Mareev, S. Electrochemical oxidation of organic pollutants in aqueous solution using a Ti_4O_7 particle anode. *Membranes* **2023**, *13*, 521. [CrossRef] [PubMed]
33. Cuesta-Mota, D.; Serra-Clusellas, A.; Macanás, J.; Canals-Casals, L.; López-Grimau, V. Electrochemical system for simultaneous treatment of textile dyeing effluents and hydrogen recovery. *Environ. Res.* **2026**, *293*, 123713. [CrossRef] [PubMed]
34. dos Santos, A.J.; Shen, H.; Lanza, M.R.; Li, Q.; Garcia-Segura, S. Electrochemical oxidation of surfactants as an essential step to enable greywater reuse. *Environ. Technol. Innov.* **2024**, *34*, 103563. [CrossRef] [PubMed]
35. Reiß, L.; Machill, S.; Lübken, T.; Herm, C. HPLC–HR-ESI–MS/MS identification of fluorescent dyes and optical brighteners and their degradation products in daylight fluorescent paints. *Herit. Sci.* **2023**, *11*, 146. [CrossRef]
36. Abo-Ayad, Z.A.; Hussein, M.F.; Zayed, M.A.; Abdelraheem, O.H. GC–MS identification of DR31 textile dye degradation products during its efficient electrochemical removal from wastewater media. *J. Mol. Liq.* **2024**, *400*, 124408. [CrossRef]
37. Pérez-Estrada, L.; Maldonado, M.; Gernjak, W.; Agüera, A.; Fernández-Alba, A.; Ballesteros, M.; Malato, S. Decomposition of diclofenac by solar driven photocatalysis at plant scale: Identification of main intermediates and degradation pathway. *Catal. Today* **2005**, *101*, 219–226. [CrossRef]
38. Wang, R.; Cao, J.; Song, J.; Liu, J.; Zhang, Y. Application of boron doped diamond for electro-Fenton and photoelectro-Fenton decolorization of azo dye from dye-containing wastewater: Acid Red 1. *Int. J. Electrochem. Sci.* **2022**, *17*, 220249. [CrossRef]
39. Sandoval, M.A.; Calzadilla, W.; Salazar, R. Influence of reactor design on the electrochemical oxidation and disinfection of wastewaters using boron-doped diamond electrodes. *Curr. Opin. Electrochem.* **2022**, *33*, 100939. [CrossRef]
40. Gao, Q.; Ding, J.; Zhao, G.; Zhao, Q.; Li, L.; Zhao, X.; Bu, L.; Zhou, S.; Qiu, S. Exploring the synergism of sunlight and electrooxidation on persulfate activation for efficient degradation of bisphenol S: Performance, Pathway, and mechanism. *Chem. Eng. J.* **2022**, *437*, 135318. [CrossRef]
41. Tang, Y.; He, D.; Guo, Y.; Qu, W.; Shang, J.; Zhou, L.; Pan, R.; Dong, W. Electrochemical oxidative degradation of X-6G dye by boron-doped diamond anodes: Effect of operating parameters. *Chemosphere* **2020**, *258*, 127368. [CrossRef] [PubMed]
42. Xu, T.; Tang, X.; Qiu, M.; Lv, X.; Shi, Y.; Zhou, Y.; Xie, Y.; Naushad, M.; Lam, S.S.; Ng, H.S.; et al. Degradation of levofloxacin from antibiotic wastewater by pulse electrochemical oxidation with BDD electrode. *J. Environ. Manag.* **2023**, *344*, 118718. [CrossRef] [PubMed]
43. Liu, F.; Oturan, N.; Zhang, H.; Oturan, M.A. Soil washing in combination with electrochemical advanced oxidation for the remediation of synthetic soil heavily contaminated with diesel. *Chemosphere* **2020**, *249*, 126176. [CrossRef] [PubMed]

44. El-Monem, H.A.; Mahanna, H.; El-Halwany, M.; Samy, M. Photo-thermal activation of persulfate for the efficient degradation of synthetic and real industrial wastewaters: System optimization and cost estimation. *Environ. Sci. Pollut. Res.* **2024**, *31*, 24153–24162. [CrossRef] [PubMed]
45. Kang, Y.; Gu, Z.; Ma, B.; Zhang, W.; Sun, J.; Huang, X.; Hu, C.; Choi, W.; Qu, J. Unveiling the spatially confined oxidation processes in reactive electrochemical membranes. *Nat. Commun.* **2023**, *14*, 6590. [CrossRef] [PubMed]
46. Qin, X.; Cao, P.; Quan, X.; Zhao, K.; Chen, S.; Yu, H.; Su, Y. Highly efficient hydroxyl radicals production boosted by the atomically dispersed Fe and Co sites for heterogeneous electro-fenton oxidation. *Environ. Sci. Technol.* **2023**, *57*, 2907–2917. [CrossRef] [PubMed]
47. Liu, D.; Chen, D.; Jiang, L.; Hao, Z.; Tan, R.; Deng, B.; Wang, Y.; Tian, Y.; Chen, L.; Jia, B. Efficient degradation of sulfamethoxazole in heterogeneous Electro-Fenton process with CeO2@MoS2@GF modified cathode: Mechanism and degradation pathway. *Sep. Purif. Technol.* **2023**, *320*, 124212. [CrossRef]
48. Wang, A.; Jiang, Y.; Yan, Y.; Bu, L.; Wei, Z.; Spinney, R.; Dionysiou, D.D.; Xiao, R. Mechanistic and quantitative profiling of electro-Fenton process for wastewater treatment. *Water Res.* **2023**, *235*, 119838. [CrossRef] [PubMed]
49. Bugueño-Carrasco, S.; Monteil, H.; Toledo-Neira, C.; Sandoval, M.Á.; Thiam, A.; Salazar, R. Elimination of pharmaceutical pollutants by solar photoelectro-Fenton process in a pilot plant. *Environ. Sci. Pollut. Res.* **2020**, *28*, 23753–23766. [CrossRef] [PubMed]
50. Brillas, E.; Garcia-Segura, S. Solar photoelectro-Fenton degradation of Acid Orange 7 azo dye in a solar flow plant: Optimization by response surface methodology. *Water Conserv. Sci. Eng.* **2016**, *1*, 83–94. [CrossRef]
51. Rabaaoui, N.; Guesmi, A.; Jabeur, W.; Mhadhbi, N.; Ben Hamadi, N.; Khezami, L.; Cherif, M.; Naïli, H. High-efficiency electro-Fenton mineralization of triclosan using a novel octahedral iron(III) complex: Structure, mechanism, and performance. *RSC Adv.* **2026**, *16*, 19687–19701. [CrossRef] [PubMed]
52. Dramou, B.J.; Shah, V.; Pinto, J.M. A kinetic model for microbial decontamination of water based on a modified Fenton reaction. *Energy Environ. Sci.* **2008**, *1*, 395–402. [CrossRef]
53. Espinoza, L.C.; Candia-Onfray, C.; Vidal, J.; Salazar, R. Influence of the chemical nature of Boron-Doped diamond anodes on wastewater treatments. *Curr. Opin. Solid State Mater. Sci.* **2021**, *25*, 100963. [CrossRef]
54. Wang, X.; Dou, J.; Deng, Z.; Gong, M.; Zhou, K.; Ma, L.; Wei, Q. Three-dimensional porous SiC/BDD electrode with long-term robustness and enhanced electrochemical degradation performance for refractory organic pollutants. *Chem. Eng. J.* **2024**, *499*, 156454. [CrossRef]
55. Partida-Joya, D.K.; Ornelas-Soto, N.; Medina-Ramírez, I.E.; Rodríguez, O.; Feria-Reyes, R.; Peralta-Hernández, J.M. Metal oxide electrode-based treatment of industrial dyes with assessment of performance and oxidation efficiency. *Processes* **2026**, *14*, 987. [CrossRef]
56. Kuchtová, G.; Hojová, L.; Staňová, A.V.; Marton, M.; Vrška, M.; Behúl, M.; Michniak, P.; Vojs, M.; Dušek, L. The influence of micro-/macro-structure of a boron-doped diamond electrode on the degradation of azo dye Direct Red 80. *Electrochim. Acta* **2023**, *464*, 142924. [CrossRef]

Disclaimer/Publisher's Note: The statements, opinions and data contained in all publications are solely those of the individual author(s) and contributor(s) and not of MDPI and/or the editor(s). MDPI and/or the editor(s) disclaim responsibility for any injury to people or property resulting from any ideas, methods, instructions or products referred to in the content.